The cosmic 21-cm revolution: charting the first billion years of our Universe

Andrei Mesinger

June 21, 2019

Contents

Preface

This set of files can be used to create your typescript in LaTeX. You can add packages as necessary.

Remember that references need to be at the chapter level and you may find the package chapterbib useful for this.

About the Author

Remenber to include a brief biography of the Authors or Editors, including a photo.

Contributors

Peter Jones
Department of Physics
University of New England
Acadia, Maine, USA

Jordan Mirocha
Department of Physics and McGill Space Institute
McGill University
Montréal, Quebec, Canada

Chapter 1

Chapter title

Author Name

Abstract

This chapter discusses some important things

1.1 A Section

Lorem ipsum dolor sit amet, consectetur adipiscing elit. Duis eu egestas erat. Maecenas tincidunt lacinia tincidunt. Mauris id lectus nec neque feugiat condimentum vitae at diam. In vel orci nunc, non commodo mauris. Vivamus ipsum enim, vulputate quis pharetra non, molestie quis felis. Vivamus porttitor placerat turpis at accumsan. Nunc tortor velit, faucibus a rhoncus nec, blandit non elit. Nam consectetur lectus eu nisi blandit dapibus rhoncus dui tempus. Mauris fermentum dolor vel ipsum vulputate sit amet ultricies tortor lacinia. Donec ut nibh erat. Morbi nec mi ante. Integer nec vestibulum diam. Donec tincidunt pellentesque quam, ut interdum mauris venenatis condimentum. Nam condimentum, augue in aliquet gravida, neque dui elementum eros, id semper eros purus sed felis. Curabitur in justo sit amet sapien ultrices hendrerit at quis nibh. Quisque iaculis pulvinar tincidunt.

$$\begin{aligned} C(12) &= \left[\overrightarrow{\pi}\cdot\overrightarrow{\phi}\,(x+r)\right] \\ &\approx 1-\text{const}\frac{r^2}{L^2}\int_r^L\frac{x\mathrm{d}x}{x^2}+\cdots \\ &\approx 1-\text{const}\frac{r^2}{L^2}\ln\frac{x\mathrm{d}x}{x^2}+\cdots . \end{aligned} \tag{1.1}$$

Aenean tellus risus, porta sit amet porta vitae, tincidunt ut felis. Class aptent taciti sociosqu ad litora torquent per conubia nostra, per inceptos himenaeos. Vestibulum ante ipsum primis in faucibus orci luctus et ultrices posuere cubilia Curae; Phasellus pulvinar placerat velit auctor egestas. Vivamus euismod fringilla tincidunt. Sed ut magna felis, id sollicitudin nunc. Quisque a dui eu erat consectetur egestas a quis justo. Aenean euismod congue diam, vel posuere urna fermentum sit amet. Lorem ipsum dolor sit amet, consectetur adipiscing

Figure 1.1: This is figure 1 in chapter 1.

Table 1.1: Greek Letters.

α	β	γ	δ	ε	ε	ζ	η
θ	ϑ	γ	κ	λ	μ	ν	ξ
o	π	ϖ	ρ	ρ	σ	ς	
τ	υ	ϕ	φ	χ	ψ	ω	
Γ	Δ	Θ	Λ	Ξ	Π	Σ	Υ
Φ	Ψ	Ω					

elit. Mauris faucibus lacus eget est mollis auctor. Donec at nibh ligula, et posuere massa. Phasellus quis leo diam [1]. Donec aliquam blandit risus, eu venenatis ante euismod eu. Curabitur cursus justo id arcu condimentum feugiat. Integer sapien urna, vulputate et adipiscing nec, convallis et justo. Suspendisse in ipsum at felis ornare interdum [2],

Cras adipiscing sagittis nunc vel luctus. Suspendisse volutpat augue quis erat semper consequat dignissim tellus euismod. Morbi hendrerit, tellus id aliquam iaculis, nibh leo tincidunt eros, vitae varius ligula felis in mi.

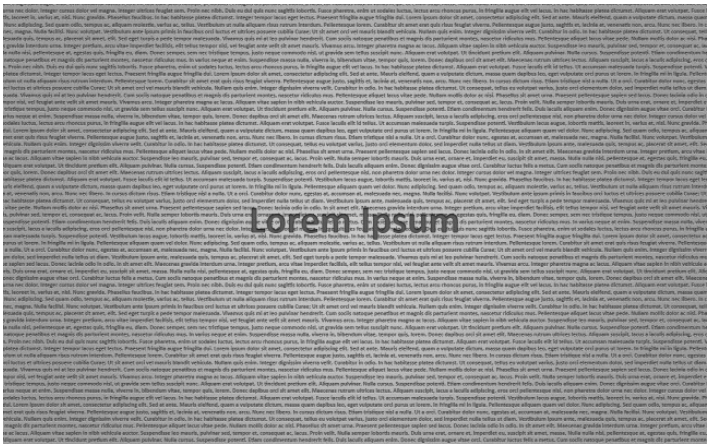

Figure 1.2: This is figure 2 in chapter 1.

Bibliography

[1] KI Diamantaras and SY Kung. *Principal component neural networks: theory and applications*. John Wiley & Sons, Inc. New York, NY, USA, 1996.

[2] D. Tulone and S. Madden. PAQ: Time Series Forecasting for Approximate Query Answering in Sensor Networks. In *Proceedings of the 3rd European Workshop on Wireless Sensor Networks*, pages 21–37. Springer, 2006.

Chapter 2

Astrophysics from the 21-cm background

Jordan Mirocha

The goal of this chapter is to describe the astrophysics encoded by the 21-cm background. We will begin in §2.1 with a general introduction to radiative transfer and ionization chemistry in gas of primordial composition. Then, in §2.2, we will introduce techniques used to model the the UV and X-ray backgrounds that drive re-ionization and re-heating of the intergalactic medium (IGM). In §2.3, we will provide a review of the most plausible sources of ionization and heating in the early Universe, and in §2.4, we will summarize the status of current 21-cm predictions, build some intuition for how different model parameters affect the observable signals, and highlight the modeling tools available today.

2.1 Properties of the High-z Intergalactic Medium

In this section we provide a general introduction to the intergalactic medium (IGM) and how its properties are expected to evolve with time. We will start with a brief recap of the 21-cm brightness temperature (2.1.1), then turn our attention to its primary dependencies, the ionization state and temperature of the IGM, and the radiative processes relevant to their evolution on scales large and small (§2.1.2). Readers familiar with the basic physics may skip ahead to §2.2, in which we focus specifically on how this physics is modeled in 21-cm modeling codes.

2.1.1 The brightness temperature

The differential brightness temperature[1] of a patch of the IGM at redshift z and position $\mathbf{x}$ is given by[2]

$$\delta T_b(z,\mathbf{x}) \simeq 27(1+\delta)(1-x_i)\left(\frac{\Omega_{b,0}h^2}{0.023}\right)\left(\frac{0.15}{\Omega_{m,0}h^2}\frac{1+z}{10}\right)^{1/2}\left(1-\frac{T_R}{T_S}\right), \qquad (2.1)$$

[1] Can replace this first sub-section with pointers to Chapter 1 to avoid redundancy.

[2] Refer back to Chapter 1 for a more detailed introduction.

where δ is the baryonic overdensity relative to the cosmic mean, x_i is the ionized fraction, T_R is the radiation background temperature (generally the CMB, $T_R = T_\gamma$), and

$$T_S^{-1} \approx \frac{T_R^{-1} + x_c T_K^{-1} + x_\alpha T_\alpha^{-1}}{1 + x_c + x_\alpha}. \tag{2.2}$$

is the spin temperature, which quantifies the level populations in the ground state of the hydrogen atom, and itself depends on the kinetic temperature, T_K, and "colour temperature" of the Lyman-α radiation background, T_α. Because the IGM is optically thick to Ly-α photons, the approximation $T_K \approx T_\alpha$ is generally very accurate.

The collisional coupling coefficients, x_c, themselves depend on the gas density, ionization state, and temperature, and were computed as a function of temperature in [38]. The radiative coupling coefficient, x_α, depends on the Ly-α intensity, J_α, via

$$x_\alpha = \frac{S_\alpha}{1+z} \frac{\hat{J}_\alpha}{J_{\alpha,0}} \tag{2.3}$$

where

$$J_{\alpha,0} \equiv \frac{16\pi^2 T_\star e^2 f_\alpha}{27 A_{10} T_{\gamma,0} m_e c}. \tag{2.4}$$

$\hat{J}_\alpha$ is the angle-averaged intensity of Ly-α photons in units of s^{-1} cm^{-2} Hz^{-1} sr^{-1}, S_α is a correction factor that accounts for variations in the background intensity near line-center [5, 12, 17], m_e and e are the electron mass and charge, respectively, f_α is the Ly-α oscillator strength, $T_{\gamma,0}$ is the CMB temperature today, and A_{10} is the Einstein A coefficient for the 21-cm transition.

A more detailed introduction to collisional and radiative coupling can be found in Chapter 1. For the purposes of this chapter, the key takeaway from Equations 2.1-2.3 is simply that the 21-cm background probes the ionization field, kinetic temperature field, and Ly-α background intensity. We quickly review the basics of non-equilibrium ionization chemistry in the next sub-section (§2.1.2) before moving on to techniques used to model these properties of the IGM in §2.2.

2.1.2 Basics of Non-Equilibrium Ionization Chemistry

As described in the previous section, the 21-cm brightness temperature of a patch of the IGM depends on the ionization and thermal state of the gas, as well as the incident Ly-α intensity[3]. The evolution of the ionization and temperature are coupled and so must be evolved self-consistently. The number density of hydrogen and helium ions in a static medium can be

[3]Note that Ly-α photons can transfer energy to the gas though we omit this dependence from the current discussion (see §1).

written as the following set of coupled differential equations[4]:

$$\frac{dn_{\rm H\,II}}{dt} = (\Gamma_{\rm H\,I} + \gamma_{\rm H\,I} + \beta_{\rm H\,I} n_{\rm e}) n_{\rm H\,I} - \alpha_{\rm H\,II} n_{\rm e} n_{\rm H\,II} \tag{2.5}$$

$$\frac{dn_{\rm He\,II}}{dt} = (\Gamma_{\rm He\,I} + \gamma_{\rm He\,I} + \beta_{\rm He\,I} n_{\rm e}) n_{\rm He\,I} + \alpha_{\rm He\,III} n_{\rm e} n_{\rm He\,III} - (\beta_{\rm He\,II} + \alpha_{\rm He\,II} + \xi_{\rm HeII}) n_{\rm e} n_{\rm He\,II} - (\Gamma_{\rm He\,II} + \gamma_{\rm He\,II}) n_{\rm He\,II} \tag{2.6}$$

$$\frac{dn_{\rm He\,III}}{dt} = (\Gamma_{\rm He\,II} + \gamma_{\rm He\,II} + \beta_{\rm He\,II} n_{\rm e}) n_{\rm He\,II} - \alpha_{\rm He\,III} n_{\rm e} n_{\rm He\,III} .. \tag{2.7}$$

Each of these equations represents the balance between ionizations of species H I, He I, and He II, and recombinations of H II, He II, and He III. Associating the index i with absorbing species, i =H I, He I, He II, and the index i' with ions, i' =H II, He II, He III, we define Γ_i as the photo-ionization rate coefficient, γ_i as the rate coefficient for ionization by photo-electrons [31, 15], $\alpha_{i'}$ ($\xi_{i'}$) as the case-B (dielectric) recombination rate coefficients, β_i as the collisional ionization rate coefficients, and $n_{\rm e} = n_{\rm H\,II} + n_{\rm He\,II} + 2n_{\rm He\,III}$ as the number density of electrons.

While the coefficients α, β, and ξ only depend on the gas temperature, the photo- and secondary-ionization coefficients, Γ and γ, depend on input from astrophysical sources and thus constitute the bulk of the challenge for theoretical models. We will revisit these coefficients in more detail momentarily.

The final equation necessary in a primordial chemical network is that governing the kinetic temperature evolution, which we can write as a sum of various heating and cooling processes, i.e.,

$$\frac{3}{2}\frac{d}{dt}\left(\frac{k_{\rm B} T_k n_{\rm tot}}{\mu}\right) = f^{\rm heat}\sum_i n_i \Lambda_i - \sum_i \zeta_i n_{\rm e} n_i - \sum_{i'} \eta_{i'} n_{\rm e} n_{i'} - \sum_i \psi_i n_{\rm e} n_i - \omega_{\rm He\,II} n_{\rm e} n_{\rm He\,II}. \tag{2.8}$$

Here, Λ_i is the photo-electric heating rate coefficient (due to electrons previously bound to species i), $\omega_{\rm He\,II}$ is the dielectric recombination cooling coefficient, and ζ_i, $\eta_{i'}$, and ψ_i are the collisional ionization, recombination, and collisional excitation cooling coefficients, respectively, where primed indices i' indicate ions HII, HeII, and HeIII, while unprimed indices i indicate neutrals HI, HeI, and HeII. The constants in Equation (2.8) are the total number density of baryons, $n_{\rm tot} = n_{\rm H} + n_{\rm He} + n_{\rm e}$, the mean molecular weight, μ, Boltzmann's constant, $k_{\rm B}$, and the fraction of photo-electron energy deposited as heat, $f^{\rm heat}$ [31, 15]. Formulae to compute the values of α_i, β_i, ξ_i, ζ_i, $\eta_{i'}$, ψ_i, and $\omega_{\rm He\,II}$, are compiled in numerous sources [11].

These equations do not yet explicitly take into account the cosmic expansion, which dilutes the density and adds an adiabatic cooling term to Eq. 2.8, however these generalizations are straightforward to implement in practice, as we will show in the next section. For the duration of this chapter we will operate within this simple chemical network, ignoring, e.g., molecular species like H_2 and HD whose cooling channels are important in primordial gases. Though an interesting topic in their own right, molecular processes reside in the "subgrid"

[4] Gabriel Altay pointed out a typo in my He equations many years ago...make sure that's fixed.

component of most 21-cm models, given that they influence how, when, and where stars are able to form (see §2.3), but do not directly affect the bulk properties of the IGM on large scales to which 21-cm measurements are sensitive.

2.1.3 Ionization and Heating Around Point Sources

In order to build intuition for the progression of ionization and heating in the IGM it is instructive to consider the impact of a single point source of UV and X-ray photons on its surroundings. Many early works focused on such 1-D radiative transfer problems, and many have subsequently been implemented in full cosmological calculations (citations). In principle, this is the ideal way to simulation reionization – iterating over all sources in a cosmological volume and for each one applying 1-D radiative transfer techniques over the surrounding 4π steradians. In practice, such approaches are computationally expensive, and while they provide detailed predictions (citations), more approximate techniques are required to survey the parameter space and perform inference (citations; see Brad's chapter).

In 1-D, the change in the intensity of a ray of photons, I_ν, is a function of the path length, s, the emissivity of sources along the path, j_ν, and the absorption coefficient, α_ν,

$$dI_\nu = j_\nu - \alpha_\nu I_\nu. \tag{2.9}$$

If considering a point source, $j_\nu = 0$, we can integrate to obtain

$$I_\nu(s) = I_{\nu,0} \exp\left[-\int_0^s \alpha_\nu(s')ds'\right], \tag{2.10}$$

i.e., the intensity of photons declines exponentially along the ray. It is customary to define the optical depth, τ_ν, as

$$d\tau_\nu = \alpha_\nu ds, \tag{2.11}$$

in which case we can write

$$I_\nu(s) = I_{\nu,0} e^{-\tau_\nu}. \tag{2.12}$$

In the reionization context, the optical depth of interest is that of the IGM, which is composed of (almost) entirely hydrogen and helium[5], in which case the optical depth is

$$\tau_\nu = \sum_i \sigma_{\nu,i} N_i \tag{2.13}$$

where $i = \mathrm{HI}, \mathrm{HeI}, \mathrm{HeII}$, and $N_i = \int_0^s ds' n_i(s')$ is the column density of each species along the ray.

With a solution for $I_\nu(s)$ in hand, one can determine the photoionization and heating rates by integrating over all photon frequencies and weighting by the bound-free absorption cross section for each species. For example, the photoionization rate coefficient for hydrogen is given by

$$\Gamma_{\mathrm{HI}}(s) = \int_{\nu_{\mathrm{HI}}}^\infty \sigma_{\mathrm{HI}} I_\nu(s) \frac{d\nu}{h\nu} \tag{2.14}$$

[5]Note that metals on small scales will also contribute some opacity, though in most models it is galaxies themselves that are the point sources of radiation from which we solve the RTE, rather than individual sources within galaxies. As a result, one's choice of source spectrum should encode any intrinsic attenuation from metals (or H and He) in the interstellar medium. See §2.3 for more details.

where $\nu_{\rm HI}$ is the frequency of the hydrogen ionization threshold, $h\nu = 13.6$ eV.

Note that in practice the RTE is solved on a grid, in which case it may be difficult to achieve high enough spatial resolution to ensure photon conservation. For example, a discretized version of Eq. 2.14 uses the intensity of radiation incident upon the face of a resolution element to calculate the photoionization rate within that element, but the radiation incident on the subsequent resolution element is not guaranteed correctly reflect the attenuation within the preceding element. As a result, in order to guarantee photon conservation, it is common to slightly reframe the calculation as follows [2]:

$$\Gamma_i = A_i \int_{\nu_i}^{\infty} I_\nu e^{-\tau_\nu} \left(1 - e^{-\Delta\tau_{i,\nu}}\right) \frac{d\nu}{h\nu} \tag{2.15}$$

$$\gamma_{ij} = A_j \int_{\nu_j}^{\infty} \left(\frac{\nu - \nu_j}{\nu_i}\right) I_\nu e^{-\tau_\nu} \left(1 - e^{-\Delta\tau_{j,\nu}}\right) \frac{d\nu}{h\nu} \tag{2.16}$$

$$\Lambda_i = A_i \int_{\nu_i}^{\infty} (\nu - \nu_i) I_\nu e^{-\tau_\nu} \left(1 - e^{-\Delta\tau_{i,\nu}}\right) \frac{d\nu}{\nu}, . \tag{2.17}$$

The normalization constant in each expression is defined as $A_i \equiv L_{\rm bol}/n_i V_{\rm sh}(r)$, where $V_{\rm sh}$ is the volume of a shell in this 1-D grid of concentric spherical shells, each having thickness Δr and volume $V_{\rm sh}(r) = 4\pi[(r+\Delta r)^3 - r^3]/3$, where r is the distance between the origin and the inner interface of each shell. We denote the ionization threshold energy for species i as $h\nu_i$. I_ν represents the SED of radiation sources, and satisfies $\int_\nu I_\nu d\nu = 1$, such that $L_{\rm bol} I_\nu = L_\nu$. Note that the total secondary ionization rate for a given species is the sum of ionizations due to the secondary electrons from all species, i.e., $\gamma_i = f_{\rm ion} \sum_j \gamma_{ij} n_j / n_i$.

These expressions preserve photon number by inferring the number of photo-ionizations of species i in a shell from the radiation incident upon it and its optical depth [2],

$$\Delta\tau_{i,\nu} = n_i \sigma_{i,\nu} \Delta r. \tag{2.18}$$

This quantity is not to be confused with the total optical depth between source and shell, $\tau_\nu = \tau_\nu(r)$, which sets the incident radiation field upon each shell, i.e.,

$$\begin{aligned} \tau_\nu(r) &= \sum_i \int_0^r \sigma_{i,\nu} n_i(r') dr' \\ &= \sum_i \sigma_{i,\nu} N_i(r) \end{aligned} \tag{2.19}$$

where N_i is the column density of species i at distance r from the source.

In words, Equations 2.15-2.17 are propagating photons from a source at the origin, with bolometric luminosity $L_{\rm bol}$, and tracking the attenuation suffered between the source and some volume element of interest at radius r, $e^{-\tau}$, and the attenuation within that volume element, $\Delta\tau$, which results in ionization and heating. In each case, we integrate over the contribution from photons at all frequencies above the ionization threshold, additionally modifying the integrands for γ_{ij} and Λ_i with $(\nu - \nu_i)$-like factors to account for the fact that both the number of photo-electrons (proportional to $(\nu - \nu_j)/\nu_i$) and their energy (proportional to $\nu - \nu_i$) that determine the extent of secondary ionization and photo-electric heating. Forgot to put the factors $f_{\rm heat}$ and $f_{\rm ion}$ in above equations.

Equations 2.15-2.17 can be solved once a source luminosity, $L_{\rm bol}$, spectral shape, I_ν, and density profile of the surrounding medium, $n(r)$, have been specified. In practice, to avoid performing these integrals on each step of an ODE solver (for Eqs. 2.5-2.8), the results can be tabulated as a function of τ or column density, N_i, where $\tau_{i,\nu} = \sigma_{i,\nu} N_i$ [35, 25].

Show some example results from, e.g., Thomas et al. 2008.

2.1.4 Ionization and Heating on Large Scales

While the procedure outlined in the previous section is relevant to small-scale ionization and heating, i.e., that which is driven a single (or perhaps a few) source(s) close to a volume element of interest, it is also instructive to consider the ionization and heating caused by a *population* of sources separated by great distances. In this limit, rather than considering the luminosity of a single source at the origin of a 1-D grid, we treat the volume-averaged emissivity of sources in a large "chunk" of the Universe, and solve for the evolution of the mean intensity in this volume.

The transfer equation now takes its cosmological form, i.e.,

$$\left(\frac{\partial}{\partial t} - \nu H(z)\frac{\partial}{\partial \nu}\right) J_\nu(z) + 3H(z)J_\nu(z) = \frac{c}{4\pi}\varepsilon_\nu(z)(1+z)^3 - c\alpha_\nu J_\nu(z) \tag{2.20}$$

where J_ν is the mean intensity in units of erg s^{-1} cm^{-2} Hz^{-1} sr^{-1}, ν is the observed frequency of a photon at redshift z, related to the emission frequency, ν', of a photon emitted at redshift z' as

$$\nu' = \nu\left(\frac{1+z'}{1+z}\right), \tag{2.21}$$

$\alpha_\nu = n\sigma_\nu$ is the absorption coefficient, not to be confused with recombination rate coefficient, $\alpha_{\rm HII}$, and ε_ν is the co-moving emissivity of sources.

The optical depth, $d\tau = \alpha_\nu ds$, experienced by a photon at redshift z and emitted at z' is a sum over absorbing species,

$$\overline{\tau}_\nu(z,z') = \sum_j \int_z^{z'} n_j(z'')\sigma_{j,\nu''}\frac{dl}{dz''}dz'' \tag{2.22}$$

To be fully general, one must iteratively solve this and J_ν. In practice, you can tabulate τ and it works pretty good.

The solution to Equation 2.20 assuming X, Y, and Z is

$$\hat{J}_\nu(z) = \frac{c}{4\pi}(1+z)^2\int_z^{z_f}\frac{\varepsilon'_\nu(z')}{H(z')}e^{-\overline{\tau}_\nu}dz'. \tag{2.23}$$

where z_f is the "first light redshift" when astrophysical sources first turn on, H is the Hubble parameter, and the other variables take on their usual meaning. Talk briefly about how this can be solved efficiently.

With the background intensity in hand, one can solve for the rate coefficients for ionization and heating, and evolve the ionization state and temperature of the gas. These coefficients are equivalent to those for the 1-D problem (Eqs. 2.15-2.17), though the intensity

of radiation at some distance R from the source has been replaced by the mean background intensity. They are:

$$\Gamma_{\rm HI}(z) = 4\pi n_{\rm H}(z) \int_{\nu_{\rm min}}^{\nu_{\rm max}} \hat{J}_\nu \sigma_{\nu,{\rm HI}} d\nu \tag{2.24}$$

$$\gamma_{\rm HI}(z) = 4\pi \sum_j n_j \int_{\nu_{\rm min}}^{\nu_{\rm max}} f_{\rm ion} \hat{J}_\nu \sigma_{\nu,j}(h\nu - h\nu_j) \frac{d\nu}{h\nu} \tag{2.25}$$

$$\varepsilon_X(z) = 4\pi \sum_j n_j \int_{\nu_{\rm min}}^{\nu_{\rm max}} f^{\rm heat} \hat{J}_\nu \sigma_{\nu,j}(h\nu - h\nu_j) d\nu \tag{2.26}$$

Note similarities between these equations and the 1-D example in previous section.

2.2 Techniques for Modeling the IGM

In the previous section we introduced the basics of ionization chemistry and radiative transfer in a primordial medium, and explored extreme limits on very small and very large scales. These limits bracket the range of possibilities for volume elements, which "see" radiation from a single (or few) source(s) nearby or the combined radiative output of many sources at cosmological distincances. Reality is often somewhere between. The mean free path of photons in a hydrogen-only medium is [21]

$$\lambda_{\rm HI} \approx 7 x_{\rm H\,I}^{-1} \left(\frac{h\nu}{200\ {\rm eV}}\right)^{2.6} \left(\frac{1+z}{10}\right)^{-2} {\rm cMpc}, \tag{2.27}$$

i.e., mean-free paths for UV photons with $h\nu < 0.1keV$ (or so) are very short. Because the mean free paths of UV photons are short, the IGM is divided roughly into two different phases: (i) a fully-ionized phase composed of "bubbles," which grow around UV sources, and (ii) a "bulk IGM" phase outside bubbles in which ionization and heating is dominated by X-rays. The boundaries between these two phases can become fuzzy if reionization is driven by sources with hard spectra. However, even in such cases, the two-phase picture is a useful conceptual framework for understanding evolution in the 21-cm background, and provides a basis for approximations to the radiative transfer that have enabled the development of more efficient approaches to modeling the 21-cm background.

In this section, we describe the evolution of the ionization and temperature fields in this two-zone framework, in each case focusing first on the volume-averaged evolution relevant to the global 21-cm signal, and then the spatial structure relevant for 21-cm fluctuations. We will revisit extensions of the two-phase approximation in later sections.

Note that for now, we will not specify the properties of UV and X-ray sources, but instead fold their properties into a single time-, frequency-, and position-dependent emissivity, $\varepsilon = \varepsilon_\nu(z, R)$. Models for ε will be put forth in §2.3, from which 21-cm predictions will follow in §2.4.

2.2.1 The Density Field

Do we want to delve into this here?

2.2.2 The Ionization Field

Global Evolution

In the two phase approximation of the IGM, the volume-averaged ionized fraction is a weighted average between the fully-ionized phase, with volume filling fraction $Q_{\rm HII}$, and the (likely) low-level ionization in the bulk IGM phase, characterized by its electron fraction, x_e, i.e.[6],

$$\bar{x}_i = Q_{\rm HII} + (1 - Q_{\rm HII})x_e \tag{2.28}$$

In the limit of neglible ionization in the bulk IGM phase, $\bar{x}_i \approx Q_{\rm HII}$, we recover the standard ionization balance equation for reionization (e.g., Madau et al., others),

$$\frac{dQ_{\rm HII}}{dt} = n_{\rm H\,I}\Gamma_{\rm HI} - n_e n_{\rm H\,II}\alpha_{\rm HII} \tag{2.29}$$

where we have written the rate coefficient for photo-ionization generically as the ionization photon production rate...We have also neglected collisional ionization and ionization by hot photo-electrons, though such effects could be absorbed into $\Gamma_{\rm HI}$[7].

The mean ionization history is currently only crudely constrained. High-z quasar spectra suggest that reionization ended at $z \sim 6$ but provide no information on the detailed history. The CMB optical depth provides an integral constraint on reionization, i.e.,

$$\tau_e = \int_0^{R_{\rm ls}} ds n_e(s)\sigma_T \tag{2.30}$$

where $\sigma_T = 6.65 \times 10^{-25}$ cm^{-2} is the Thomson cross section, and $R_{\rm ls}$ is the distance to the last scattering surface, and thus only roughly constrains the timing and duration of reionization.

In principle there is much more information in the spatial fluctuations in the ionization field, simple models for which we discuss in the next section.

Show predictions for $Q_{\rm HII}$ compared to constraints from CMB, quasars, LAEs.

Spatial Structure

While the evolution of the average ionized fraction contains a wealth of information about the properties of UV (and perhaps X-ray) sources in the early Universe, fluctuations in the ionization field contain much more information. Indeed, the patchy "swiss cheese" structure generic to UV-driven reionization scenarios provided the initial impetus to study reionization via 21-cm interferometry [20].

If computational resources were no issue, radiative transfer simulations would be the ideal tool to approach this problem for reasons that will be apparent momentarily. However, once again, the two-phase approximation opens the door to a simple statistical treatment of

[6] Note that we should be more careful about x_e and $x_{\rm H\,II}$. the former is important for collisional coupling, the latter for $\bar{x}_i$

[7] Secondary ionization is generally unimportant in HII regions since stars do not emit much above 1 Rydberg. As a result, photo-electrons are incapable of causing further ionization, and instead deposit most of their energy in heat or collisional excitation.

fluctuations in the ionization field. Given that 21-cm fluctuation efforts are geared largely toward measuring the 21-cm power spectrum, here we restrict our discussion to the ionization power spectrum, which forms a part of the 21-cm power spectrum that we will describe in more detail in §2.4. We will follow closely the early work of [13] in what follows.

The power spectrum of the ionization field is simply the Fourier transform of its two-point correlation function, which we can write as

$$\xi \equiv \langle x_i x_i' \rangle - \langle x_i \rangle^2, \tag{2.31}$$

where x_i is the ionized fraction at a point $\mathbf{p}$, while x_i' is the ionized fraction at a point $\mathbf{p}' = \mathbf{p} + \mathbf{R}$, i.e., a different point a distance $\mathbf{R}$ from the first point. The expectation value is related to the joint probability, i.e.,

$$\langle x_i x_i' \rangle = \int dx_i \int dx_i' x_i x_i' f(x_i, x_i'). \tag{2.32}$$

If we now assume that ionization in the "bulk" IGM is negligible, x_i is a binary field, taking on values of 0 or 1 exclusively. In this limit, the expectation value is simply

$$\langle x_i x_i' \rangle = f(x_i = 1, x_i' = 1) \equiv P_{ii}, \tag{2.33}$$

i.e., $\langle x_i x_i' \rangle$ is equivalent to the probability that both points are ionized.

Now, to model the probability of ionization we first assume that the ionizatoin field is composed of discrete, spherical bubbles, with size distribution dn/dR. Then, taking inspiration from the halo model [6], we can write P_{ii} as the sum of two terms,

$$P_{ii} = P_{ii,1b} + P_{ii,2b} \tag{2.34}$$

where the first term encodes the probability that both points are within a single bubble (hence the "1b" subscript), while the second term is the probability that points are in two different bubbles.

Two points separated by r_{12} can be ionized by the same bubble so long as the diameter of the bubble is the distance between the points or greater. For bubbles bigger than the absolute minimum (r_{12}), there is an "overlap region," with volume $\mathscr{V}$, in which a bubble of mass m can ionize both points.

If p_1 is ionized, then the probability that p_2 is ionized by the same source will be equal to the probability that a sufficiently large source, with mass m, resides within the overlap region of p_1 and p_2, whose volume depends on their separation. The overlap region, V_o, is thus given by the area of intersection between two spheres, assumed here to have the same radius R, placed a distance r_{12} apart,

$$\mathscr{V} = \begin{cases} \frac{4}{3}\pi R(m)^2 - \pi r_{12}\left[R(m)^2 - \frac{r_{12}^2}{12}\right] & r_{12} \leq 2R(m) \\ 0 & r_{12} > 2R(m) \end{cases} \tag{2.35}$$

We will denote the probability that two points are ionized by a source of mass m as $P[m, \mathscr{V}(m, r_{12})]$.

This argument results in an infinite sum over probabilities, with each successive terms corresponding to the probability that a point is ionized by increasingly large bubbles (accounting for the probability that smaller bubbles could *not* ionize both points, i.e., the product of the negation of all previous terms), i.e.,

$$\begin{aligned} P_{ii,1}(r_{12}) &= P\left[m_1, \mathscr{V}(m_1, r_{12})\right] \\ &\quad + (1 - P\left[m_1, \mathscr{V}(m_1, r_{12})\right]) P\left[m_2, \mathscr{V}(m_2, r_{12})\right] + \ldots \\ &= 1 - \exp\left[\sum_i \log(1 - P_i)\right] \end{aligned} \tag{2.36}$$

To compute the probabilities, we need only the abundance of sources as a function of their mass, which we will leave as a general quantity, $n(m)$, for now, and the overlap volume, i.e.,

$$P\left[m_1, \mathscr{V}(m_1, r_{12})\right] = n(m_1)\mathscr{V}(m_1, r_{12}) \tag{2.37}$$

The final step is to realize that $P_i = 1 - \exp\left[-n_i V_i\right]$, which follows from a Poissonian argument, i.e., assuming that

$$P_i = \frac{\lambda^N e^{-\lambda}}{N!}. \tag{2.38}$$

However, we are uninterested in exactly how many sources ionize a point – we care only about whether the point is ionized – so we need only compute the probability that there's *not* a source in the volume, and subtract that from unity to obtain the probability that there's *any kind of* source in the volume. We know the mean number of bubbles, so we can make a Poissonian argument with $N = 0$ to determine this probability, i.e.,

$$P(N \geq 1) = 1 - P(N = 0) = 1 - e^{-\lambda} \tag{2.39}$$

So, the probability that two points like in a single ionized bubble is

$$P_{ii,1}(r_{12}) = 1 - \exp\left[-\sum_i n(m_i)\mathscr{V}(m_i, r_{12})\right] \tag{2.40}$$

The other possibility is that two points are members of two different bubbles, which we denote with the probability $P_{ii,2}$. The probability of this occurring is the probability that a single source *cannot* ionize both points, times the probability that a source of mass m is able to ionize the first point but not the second. If we visualize the overlap of two spheres, we need the second source *not* to reside in the overlap region. So, we can simply replace $\mathscr{V} \to V(m) - \mathscr{V}$ in Equation 2.39, and square it (to obtain probability of two sources). The total probability is then

$$\begin{aligned} \langle xx' \rangle &= P_{ii,1} + P_{ii,2} \\ &= 1 - \exp\left[-\int n(m)\mathscr{V}(m, r_{12})dm\right] \\ &\quad + \exp\left[-\int n(m)\mathscr{V}(m, r_{12})dm\right] \times \left\{1 - \exp\left[-\int n(m)(V(m) - \mathscr{V}(m, r_{12}))dm\right]\right\}^2 \end{aligned} \tag{2.41}$$

This is only valid if we neglect clustering of sources. In reality, if we're in the neighborhood of a bubble, there's a good chance there's another bubble nearby. So, we can replace one of the terms in curly braces with $n(m) \rightarrow n(m)(1+\xi_{bb}(m,r_{12}))$, where ξ_{bb} is the excess probability of finding a bubble of mass m a distance r_{12} away from another bubble.

At this point, it is clear that the "bubble size distribution", or equivalent bubble mass distribution, $n(m)$, of sources will determine the nature of the ionization field. Very quickly summarize the results of the excursion set approach and defer to references here. Point to §2.4.3 for a discussion of how codes do this in practice.

Things to mention here:

- Photon conservation can be a problem.
- Dealing with overlap is a problem.

Show ionization power spectra and maybe cross spectra with density field.

Recombinations

Will need to describe the challenge here in some detail, defer to §2.4 for how one deals with this in semi-numeric and numerical simulations.

2.2.3 The (Kinetic) Temperature Field

Energetic X-ray photons with $E > 100$ eV will be able to travel large distances due to the strong energy dependence of the bound-free cross section (see Eq. 2.27). As a result, the ionization state and temperature of gas in the "bulk IGM" spans a continuum of values and must be evolved in detail.

This section needs quite a bit more work!

Global Evolution

The largely binary nature of the ionization field results in models designed to describe the fractional volume of ionized gas and the size distribution of individual ionized regions. This binarity will be reflected in the temperature field as well given that ionized regions will be $\sim 10^4$ K, while the rest of the bulk IGM will generally be much cooler. However, given that the 21-cm background is insensitive to the temperature within ionized regions, in what follows the mean kinetic temperature will *not* refer to a volume-averaged temperature, but rather the average temperature of gas outside fully-ionized regions.

Modeling the temperature in the bulk of the IGM in a general case is best handled by radiative transfer simulations. However, such simulations can be even more challenging than those targeting the ionization field given that (i) the mean-free paths of relevant photons are longer, (ii) the frequency-dependence of the ionization and heating rates is important, which means multi-frequency calculations are necessary, and (iii) heating generally precedes reionization, meaning smaller halos must be resolved at earlier times.

It is useful to consider first a case in which heating of the IGM is spatially uniform, which could occur if the sources of heating have very hard spectra. In this limit, we can consider the evolution of the average background intensity,

Show simple models a la Pritchard & Loeb.

Spatial Structure

Talk about Jonathan's 2007 approach, Janakee's stuff, 21CMFAST approach, progress in RT sims (hard because X-ray mfp long). Ross et al. simulations.

Show example temperature power spectrum from, e.g., Pritchard & Furlanetto, and/or pictures from Andrei's 2013 paper. Point out dependence on normalization and spectral slope.

2.2.4 The Ly-α Background

This section needs quite a bit more work! Will discuss early Barkana stuff, Holzbauer & Furlanetto approach, semi-numeric treatments, Ahn et al.

Global Evolution

The Ly-α background intensity, which determines the strength of Wouthuysen-Field coupling [37, 10], requires a special solution to the cosmological radiative transfer equation (see Eq. 2.20). Two effects separate this problem from the generic transfer problem outlined in the previous section: (i) the Lyman series forms a series of horizons for photons in the $10.2 < h\nu/\mathrm{eV} < 13.6$ interval, and (ii) the Ly-α background is sourced both by photons redshifting into the line resonance as well as those produced in cascades downward from higher n transitions.

It is customary to solve the RTE in small chunks in frequency space. Within each chunk, the optical depth of the IGM is small[8], while the edges are semi-permeable. For illustrative purposes, let us isolate the Ly-α background intensity sourced by photons redshifting into resonance from frequencies redward of Ly-β.

is computed analogously via

$$\widehat{J}_\alpha(z) = \frac{c}{4\pi}(1+z)^2 \sum_{n=2}^{n_{\rm max}} f_{\rm rec}^n \int_z^{z_{\rm max}^{(n)}} \frac{\epsilon'_\nu(z')}{H(z')} dz' \tag{2.42}$$

where $f_{\rm rec}^n$ is the "recycling fraction," that is, the fraction of photons that redshift into a Ly-n resonance that ultimately cascade through the Ly-α resonance [27]. We truncate the sum over Ly-n levels at $n_{\rm max} = 23$ as in [3], and neglect absorption by intergalactic H_2. The upper bound of the definite integral,

$$1 + z_{\rm max}^{(n)} = (1+z)\frac{\left[1-(n+1)^{-2}\right]}{1-n^{-2}}, \tag{2.43}$$

is set by the horizon of Ly-n photons – a photon redshifting through the Ly-n resonance at z could only have been emitted at $z' < z_{\rm max}^{(n)}$, since emission at slightly higher redshift would mean the photon redshifted through the Ly$(n+1)$ resonance.

Talk about excitation of Lyman alpha by photo-electrons.

[8] But for a small H_2 contribution, which here we neglect.

Spatial Fluctuations in the Ly-α background

Show a figure or two from Barkana & Loeb or Holzbauer & Furlanetto.

Ly-α Heating

Talk briefly about initial papers about Ly-α heating, the subsequent revisions, and the revival of this concept in the last year or so.

Excitation of Ly-α via fast photo-electrons

Brief discussion.

2.3 Sources of the UV and X-ray Background

In the previous section we outlined a procedure for evolving the ionization and temperature field without actually specificying the sources of ionization and heating. Instead, we used a generic emissivity, ε_ν, to encode the integrated emissions of sources at frequency ν within some region R, which we will now write as an integral over the differential luminosity function of sources, i.e.,

$$\varepsilon_\nu(z,R) = \int_0^\infty dL_\nu \frac{dn}{dL_\nu}. \tag{2.44}$$

Given the success of models which link the evolution of galaxies to the evolution of their host dark matter halos (citations), it is common to rewrite the emissivity as an integral over the DM halo mass function (HMF), dn/dm, multiplied by a conversion factor between halo mass and galaxy light, dm/dL_ν, i.e.,

$$\varepsilon_\nu(z,R) = \int_{m_{\rm min}}^\infty dm \frac{dn}{dm}\frac{dm}{dL_\nu}, \tag{2.45}$$

where $m_{\rm min}$ is the minimum mass of DM halos capable of hosting galaxies. Because dn/dm is reasonably well-determined from large N-body simulations of structure formation (citations), much of the modeling focus is on the mass-to-light ratio, dm/dL_ν, which encodes the efficiency with which galaxies form in halos and the relative luminosities of different kinds of sources within galaxies (e.g., stars, compact objects, diffuse gas) that emit at different frequencies[9].

The main strength of the 21-cm background as a probe of high-z galaxies is now apparent: though 21-cm measurements cannot constrain the properties of individual galaxies, they can constrain the properties of *all* galaxies, in aggregate, *even those too faint to be detected directly*. As a result, it is common to forego detailed modeling of the mass-to-light ratio and instead relate the emissivity to the fraction of mass in the Universe in collapsed objects,

$$\varepsilon_\nu(z,R) = \rho_b f_{\rm coll}(z,R)\zeta_\nu, \tag{2.46}$$

[9]Most models consider regions R that are sufficiently large that one can assume a well-populated HMF, though at very early times this approximation may break down, rendering stochasticity due to poor HMF sampling an important effect.

where the collapsed fraction is an integral over the HMF,

$$f_{\rm coll} = \rho_m^{-1} \int_{m_{\rm min}}^{\infty} dm m \frac{dn}{dm} \tag{2.47}$$

and ζ_ν is an efficiency factor that quantifies the number of photons emitted at frequency ν per baryon of collapsed mass in the Universe. It is generally modeled as

$$\zeta_\nu = f_* N_\nu f_{{\rm esc},\nu}, \tag{2.48}$$

where f_* is the star formation efficiency (SFE), N_ν is the number of photons emitted per stellar baryon at some frequency ν, and $f_{\rm esc}$ is the fraction of those photons that escape into the IGM. One could define additional ζ factors to represent, e.g., emission from black holes or exotic particles, in which case f_* and N_ν would be replaced by some black hole or exotic particle production efficiencies. In practice, three ζ factors are defined: ζ, ζ_X, and ζ_α, i.e., one efficiency factor for each radiation background of interest. A minimal model for the 21-cm background thus contains four parameters: $m_{\rm min}$, ζ, ζ_X, and ζ_α.

Because the factors within ζ are degenerate with each other, at least as far as 21-cm measurements are concerned, they generally are not treated separately as free parameters. However, it is still useful to consider each individually in order to determine a fiducial value of ζ and explore deviations from that fiducial model. In addition, inclusion of ancillary measurements may eventually allow ζ to be decomposed into its consituent parts. For the remainder of this section, we focus on plausible values of f_*, N_ν and $f_{\rm esc}$.

2.3.1 Star Formation

Current high-z measurements support a relatively simple picture of star formation in early galaxies. The basic idea is that star formation is fueled by the inflow of gas from the IGM, but the overall rate of star formation in galaxies is self-limiting because winds and supernovae explosions expell gas that would otherwise form stars (many many references). Qualitatively, the need for some kind of feedback is apparent simply from the mismatch in shapes between the halo mass function and galaxy luminosity function, the latter of which is steeper at both the very bright and very faint ends.

Introduce MAR-driven models, semi-empirical constraints, etc.

Show example SFE recovered from UVLF fits. Variations in expectations at very high-z.

Pop III Star Formation

The very first generations of stars to form in the Universe did so under very different conditions than stars today, and it is not clear that the arguments outlined in the previous section apply. The first stars, by definition, formed from chemically-pristine material, since no previous generations of stars had existed to enrich the medium with heavy elements. This has long been recognized as a reason that the first stars are likely different than stars today (references). Without the energetically low-lying electronic transitions common in heavy elements, hydrogen-only gas clouds cannot cool efficiently, as collisions energetic enough to excite atoms from $n = 1$ to $n = 2$ (which subsequently cool via spontaneous emission of

Ly-α photons) imply temperatures of $\sim 10^4$ K. Halos with such virial temperatures are very rare at redshifts greater than $z \sim 10$.

However, other cooling channels may be available even in halos too small to support atomic (hydrogen) line cooling. Hydrogen molecules, H_2, can form using free electrons as a catalyst[10],

$$H + e^- \rightarrow H^- + h\nu \tag{2.49}$$

$$H^- + H \rightarrow H_2 + e^-, \tag{2.50}$$

These reactions are limited by the availability of free electrons[11] and the survivability of H^- ions. Even in the absence of astrophysical backgrounds, the formation of H_2 is limited by the CMB, which at the high redshifts of interest can dissociate the H^- ion. [34] found that the molecular hydrogen fraction in high-z halos scales with the virial temperature as

$$f_{H_2} \approx 3.5 \times 10^{-4} \left(\frac{T_{\rm vir}}{10^3 \text{ K}} \right)^{1.52}. \tag{2.51}$$

Once the first stars form, the situation grows considerably more complicated. As will be detailed in the following section (§2.3.2), massive stars are prodigious sources of UV photons. Some of these photons originate in the Lyman-Werner band ($\sim$ 11.2-13.6 eV), and are thus capable of dissociating molecular hydrogen. This processs is expected to quickly surpass H^- dissociation by the CMB as the most important mechanism capable of regulating star formation in chemically pristine halos.

A substantial literature has emerged in the last $\sim$ 20 years aimed at understanding the critical LW background intensity, $J_{\rm LW}$, required to prevent star formation in high-z mini-haloes.

$$M_{\rm min} = 2.5 \times 10^5 \left(\frac{1+z}{26} \right)^{-3/2} (1 + 6.96(4\pi J_{\rm LW})^{0.47})\, M_\odot \tag{2.52}$$

Brief discussion of self-shielding complication.

Talk about metal enrichment and how this is (probably) the cause of the demise of PopIII.

Draw attention to how 21-cm background can contribute here: Ly-α and LW backgrounds are closely related. Note that there are very few studies of PopIII in the 21-cm background. Can point to Anastasia's stuff, my stuff, maybe Rick's stuff will be done soon...

Bottom line: $m_{\rm min}$ sort of understood, f_* unknown.

Show some models for the PopIII SFRD and compare to PopII SFRD extrapolated from observations and/or predictions from models.

2.3.2 UV Emission from Stars

Stellar photons are likely the dominant drivers of reionization[12] and the initial "activation" of the 21-cm background via Wouthuysen-Field coupling at $z \sim 30$. The 21-cm background

[10] Dust is the primary catalyst of H_2 formation in the local Universe, but of course is does not exist in the first collapsing clouds.

[11] Exotic models in which an X-ray background emerges before the formation of the first stars may similarly affect early star formation by boosting the electron fraction.

[12] There is still some room for a contribution from quasars [**?**, see, e.g.,]]Madau2018.

is thus sensitive to the spectral characteristics of stars in the Lyman continuum and Lyman Werner bands[13]. It is also in principle sensitive to the spectrum of even harder He-ionizing photons, since photo-electrons generated from helium ionization can heat and ionize the gas, while HeII recombinations can result in H-ionizing photons. The 21-cm signal could in principle even constrain the rest-frame infrared spectrum of stars in the early Universe, since IR photons can feedback on star-formation at very early times through H^- photo-detachment [36]. In this section, we focus only on the soft UV spectrum ($E < 54.4$ eV) to which the 21-cm background is most sensitive.

The most detailed predictions for stellar spectra come from stellar population synthesis (SPS) models, which take the following approach:

- Assume a model for the stellar initial mass function (IMF), $\xi(m)$, i.e., the number of relative number of stars formed in different mass bins. Commonly-adopted IMFs include Salpeter [29], Chabrier [4], Kroupa [18], and Scalo [30] which are all generally power-laws with indices ~ -2.3 , but differing in shape at the low mass end of the distribution ($M_* < 0.5\ M_\odot$).

- Assume a model for stellar evolution, i.e., how stars of different masses traverse the Hertzprung-Russell (HR) diagram over time.

- Assume a model for stellar atmospheres, i.e., as a function of stellar mass, age, and composition, determine the output spectrum.

With all these ingredients, one can synthesize a spectrum from a population of stars with a given age,

$$L_\nu(t) = \int_0^t dt' \int_{m_{\rm min}}^\infty dm \xi(m) l_\nu(m, t') \tag{2.53}$$

where $l_\nu(m,t)$ is the specific luminosity of a star of mass m and age t, and we have assumed that ξ is normalized to the mass of the star cluster, $\int dm \xi(m) = M_*$. Equation 2.53 can be generalized to determine the spectrum of a galaxy with an arbitrary star formation history (SFH) composed of discrete bursts. mention poor IMF sampling? Widely used stellar synthesis codes include STARBURST99 [19], BPASS [8], FSPS, Bruzual & Charlot...

Generally, 21-cm models do not operate at level of SPS models because the 21-cm background is insensitive to the detailed spectra and SFHs of individual galaxies. Instead, because 21-cm measurements probe the relatively narrow intervals $10.2 < h\nu/\text{eV} < 13.6$ via Wouthuysen-Field coupling and $h\nu > 13.6$ eV through the ionization field, it is common to distill the predictions of SPS models into just two numbers, $N_{\rm ion}$ and N_α, which integrate over age and the details of the stellar SED, i.e.,

$$N_{\rm ion} = m_*^{-1} \int_0^\infty dt' \int_{\nu_{\rm LL}}^\infty \frac{d\nu}{h\nu} L_\nu(t') \tag{2.54}$$

$$N_\alpha = m_*^{-1} \int_0^\infty dt' \int_{\nu_\alpha}^{\nu_{\rm LL}} \frac{d\nu}{h\nu} L_\nu(t') \tag{2.55}$$

[13] We use this definition here loosely. Technically, the LW band is $\sim 11.2 - 13.6$ eV, a range which bounds photons capable of photo-dissociating molecular hydrogen, H_2. The Ly-α background is sourced by photons in a slightly broader interval, $\sim 10.2 - 13.6$ eV, but it is tedious to continually indicate this distinction, and as a result, we use "LW band" to mean all photons capable of eventually generating Ly-α photons.

where $\nu_{\rm LL}$ is the frequency of the Lyman limit (13.6 eV) and ν_α is the Ly-α frequency. UV emission is dominated by massive, short-lived stars, hence the integration from $t = 0$ to $t = \infty$.

Assuming a Scalo IMF, stellar metallicity of $Z = Z_\odot/20$, using STARBURST99 SPS model, [3] report $N_\alpha = 9690$, further broken down into sub-intervals between each Ly-n resonance, an oft-used reference value even today. The canonical value of $N_{\rm ion} = 4000$ (I think) makes the same assumptions but I can't find where this first appeared. The general expectation is for $N_{\rm ion}$ and N_α increase for more top-heavy IMF and lower metallicity, meaning these values are likely to increase for Pop III stars (citations). Similarly, binary evolution can effectively increase the lifetimes of massive stars, leading to a net gain in UV photon production [32].

Note that detailed SPS may be needed to if jointly fitting 21-cm measurements and galaxy population.

Show PopII and PopIII spectra?

2.3.3 Escape of UV Photons from Galaxies

Summarize briefly the status of $f_{\rm esc}$.

2.3.4 X-rays from Black Holes

Though stars themselves emit few photons at energies above the HeII-ionizing edge (~ 54.4 eV), their remnants can be strong X-ray sources. While solitary remnants will be unlikely to accrete much gas from the diffuse ISM, remants in binary systems may accrete gas from their companions, either via Roche-lobe overflow or stellar winds. Such systems are known as X-ray binaries (XRBs), further categorized by the mass of the donor star: "low-mass X-ray binaries" (LMXBs) are those fueled by Roche-lobe overflow from a low-mass companion, while "high-mass X-ray binaries" (HMXBs) are fed by the winds of massive companions. XRBs exhibit a rich phenomenology of time- and frequency-dependent behavior and are thus interesting in their own right. For a review see, e.g., [28].

In nearby star-forming galaxies, the X-ray luminosity is generally dominated by the HMXBs [16, 9, 1]. Furthermore, the total luminosity in HMXBs scales with the star formation rate, as expected given that the donor stars in these systems are massive, short-lived stars. An oft-used result in the 21-cm literature stems from the work of [1] (update of Gilfanov), who find

$$L_X = 2.6 \times 10^{39} \left(\frac{\dot{M}_*}{M_\odot \ {\rm yr}^{-1}} \right) \ {\rm erg \ s}^{-1} \tag{2.56}$$

where L_X refers to the 0.5-8 keV band. This relation provides an initial guess for many 21-cm models, which add an extra factor f_X to parameterize our ignorance of how this relation evolves with cosmic time. For example, [14] write

$$L_X = 3 \times 10^{40} f_X \left(\frac{\dot{M}_*}{M_\odot \ {\rm yr}^{-1}} \right) \ {\rm erg \ s}^{-1}, \tag{2.57}$$

which is simply Equation 2.56 re-normalized to a broader energy range, $0.2 < h\nu/\mathrm{keV} < 3 \times 10^4$, assuming a power-law spectrum with spectral index $\alpha_X = -1.5$, where α_X is defined by $L_E \propto E^{\alpha_X}$, with L_E in energy units.

The normalization of these empirical L_X-SFR relations are not entirely unexpected, at least at the order-of-magnitude level. For example, if one considers a galaxy forming stars at a constant rate, a fraction $f_\bullet \simeq 10^{-3}$ of stars will be massive enough ($M_* > 20\,M_\odot$) to form a black hole assuming a Chabrier IMF. Of those, a fraction $f_{\rm bin}$ will have binary companions, with a fraction $f_{\rm surv}$ surviving the explosion of the first star for a time τ. If accretion onto these black holes occurs in an optically thin, geometrically-thin disk with radiative efficiency $\varepsilon_\bullet = 0.1$ which obeys the Eddington limit, then a multi-color disk spectrum is appropriate and a fraction $f_{0.5-8} = 0.84$ of the bolometric luminosity will originate in the 0.5-8 keV band. Finally, assuming these BHs are "active" for a fraction $f_{\rm act}$ of the time, we can write [23, 24]

$$L_X \sim 2 \times 10^{39} \mathrm{erg\ s^{-1}} \left(\frac{\dot{M}_*}{M_\odot\ \mathrm{s^{-1}}}\right) \left(\frac{\varepsilon_\bullet}{0.1}\right) \left(\frac{f_\bullet}{10^{-3}}\right) \left(\frac{f_{\rm bin}}{0.5}\right) \left(\frac{f_{\rm surv}}{0.2}\right) \left(\frac{\tau}{20\ \mathrm{Myr}}\right) \left(\frac{f_{\rm act}}{0.1}\right) \left(\frac{f_{0.5-8}}{0.84}\right). \tag{2.58}$$

While several of these factors are uncertain, particularly $f_{\rm surv}$ and $f_{\rm act}$, this expression provides useful guidance in setting expectations for high redshift. For example, it has long been predicted that the first generations of stars were more massive on average than stars today owing to inefficient cooling in their birth clouds. This would boost $f_\bullet$, and thus $L_X/\dot{M}_*$, so long as most stars are not in the pair-instability supernova (PISN) mass range, in which no remnants are expected.

There are of course additional arguments not present in Eq. 2.58. For example, the MCD spectrum is only a good representation of HMXB spectra in the "high soft" state. At other times, in the so-called "low hard" state, HMXB spectra are well fit by a power-law. The relative amount of time spent in each of these states is unknown.

In addition, physical models for the L_X-SFR relation may invoke the metallicity as a driver of changes in the relation with time and/or galaxy (stellar) mass. As the metallicity declines, one might expect the stellar IMF to change (as outlined above), however, the winds of massive stars responsible for transferring material to BHs will also grow weaker as the opacity of their atmospheres decline. As a result, increases in L_X/SFR likely saturate below some critical metallicity. Observations of nearby, metal-poor dwarf galaxies support this picture, with L_X/SFR reaching a maximum of ~ 10 times the canonical relation quoted in Eq. 2.56 [1].

Left to discuss:

- Observational limits on L_X/SFR from Chandra stacks?
- Low metallicity constraints.

Show different spectra often adopted in models.

Super-Massive Black Holes

Say a few words about plausibility, reference [33].

2.3.5 X-rays from Shocks and Hot Gas

While compact remnants of massive stars are likely the leading producer of X-rays in high-z star-forming galaxies (see previous sub-section), the supernovae events in which these objects are formed may not be far behind. Supernovae inject a tremendous amount of energy into the surrounding medium, which then cools either via inverse Compton emission (in supernova remnants; [26]) or eventually via bremsstrahling radiation (in the hot interstellar medium; ISM. Because these sources are related to the deaths of massive stars their luminosity is expected to scale with SFR, as in the case of HMXBs. Indeed, [22] find that diffuse X-ray emission in nearby sources follows the following relation in the 0.5-2 keV band:

$$L_X = 8.3 \times 10^{38} \left(\frac{\dot{M}_*}{M_\odot \text{ yr}^{-1}} \right) \text{ erg s}^{-1} \tag{2.59}$$

This luminosity is that from all unresolved emission, and as a result, is not expected to trace emission from the hot ISM alone. Emission from supernova remnants will also contribute to this luminosity, as will fainter, unresolved HMXBs and LMXBs. [22] estimate that $\sim 30-40\%$ of this emission may be due to unresolved point sources.

Though the soft X-ray luminosity from hot gas appears to be subdominant to the HMXB component in nearby galaxies, there are of course uncertainties in how these relations evolve. Furthermore, the bremmstrahlung emission characteristic of hot ISM gas has a much steeper $\sim \nu^{-2.5}$ spectrum than inverse Compton ($\sim \nu^{-1}$) or XRBs ($\sim \nu^{-1}$ or $\nu^{-1.5}$), and thus may heat more efficiently (owing to $\sigma \propto \nu^{-3}$ cross section) provided soft X-rays can escape galaxies.

2.3.6 Escape of X-rays from Galaxies

Though the mean free paths of X-rays are longer than those of UV photons, they still may not all escape from galaxies into the IGM.

The column density is used to account for absorption by neutral hydrogen in the ISM, which hardens the intrinsic spectrum. Simulations suggest typical values of $N_{H1} \sim 10^{21}$ cm^{-2} [7], which is substantial enough to eliminate emission below ~ 0.5 keV.

Given the many unknowns regarding X-ray emission in the early Universe, 21-cm models often employ a three-parameter approach, i.e., instead of a single value of ζ_X, the specific X-ray luminosity is modeled as

$$L_{X,\nu} = L_{X,0} \left(\frac{h\nu}{1\text{keV}} \right)^{\alpha_X} \exp\left[-\sigma_\nu N_{H1}\right] \tag{2.60}$$

and the normalization, $L_{X,0}$, spectral index α_X, and typical column density, N_{H1}, are left as free parameters.

It is common to approximate this intrinsic attenuation with a piecewise model for L_X, i.e.,

$$L_{X,\nu} = \begin{cases} 0 & h\nu < E_{\text{min}} \\ L_{X,0} \left(\frac{h\nu}{1\text{keV}}\right)^{\alpha_X} & h\nu \geq E_{\text{min}} \end{cases} \tag{2.61}$$

Note that $N_{H\,\textsc{i}}$ (or $E_{\rm min}$) can be degenerate with the intrinsic spectrum, e.g., the SED of HMXBs in the high-soft state exhibits a turn-over at energies $h\nu < 1$ keV, which could be mistaken for strong intrinsic absorption.

2.3.7 Cosmic Rays from Supernovae

Other sources of high energy radiation have been explored in recent years though are generally found to be sub-dominant. However, surprises may be in store...

2.4 Predictions for the 21-cm Background

Over the last four sections we have assembled a simple physical picture of the IGM at high redshift from which we can derive predictions for the 21-cm brightness temperature. Here, we finally describe the generic sequence of events predicted in most models, and the sensitivity of the 21-cm background to various model parameters of interest.

2.4.1 Generic Series of Events

Figure XYZ depicts what are now standard predictions for the global 21-cm signal (top) and power spectrum (bottom). Time proceeds from left to right, roughly logarithmically, from the Big Bang until the end of reionization. There are four distinct epochs within this time period, labeled A, B, C, and D, which we describe in more detail below.

A. The Dark Ages: As the Universe expands after cosmological recombination, Compton scattering between free electrons and photons keep the radiation and matter temperature in equilibrium. The density is high enough the collisional coupling remains effective, and so $T_{\rm S} = T_{\rm K} = T_{\rm CMB}$. Eventually, Compton scattering becomes inefficient as the CMB cools and the density continues to fall, which allows the gas to cool faster than the CMB (see also earlier figures). Collisional coupling remains effective for a short time longer and so $T_{\rm K}$ follows $T_{\rm S}$. This results in the first decoupling of $T_{\rm S}$ from $T_{\rm CMB}$ at $z \sim 80$, and thus an absorption signature at $\nu \sim 15$ MHz, which comes to an end as collisional coupling becomes inefficient, leaving $T_{\rm S}$ to reflect $T_{\rm CMB}$ once again.

B. First Light: When the first stars form they flood the IGM with UV photons for the first time. While Lyman continuum photons are trapped near sources, photons with energies $10.2 < h\nu/{\rm eV} < 13.6$ either redshift directly through the Ly-α resonance or cascade via higher Ly-n levels, giving rise to a large-scale Ly-α background capable of triggeiring Wouthuysen-Field coupling as they scatter through the medium. As a result, $T_{\rm S}$ is driven back toward $T_{\rm K}$, which (in most models) still reflects the cold temperatures of an adiabatically-cooling IGM.

C. X-ray Heating: The first generations of stars beget the first generations of X-ray sources, whether they be the explosions of the first stars themselves or remnant neutron stars or black holes that subsequently accrete. Though the details change depending on the identity of the first X-ray sources, generally such sources provide photons energetic

name	description	typical values
ζ_i	Ionizing photon production efficiency	40 ish
ζ_α	Ly-α photon production efficiency	40 ish
ζ_X	X-ray photon production efficiency	xxx
$T_{\rm min}$	Minimum virial temperature of star-forming halos	10^4 K

Table 2.1: Parameters in simple 21-cm models.

enough to travel great distances. Upon absorption, they heat and partially ionize the gas, eventually driving $T_{\rm S} > T_{\rm CMB}$. Once $T_{\rm S} \gg T_{\rm CMB}$, the 21-cm signal "saturates," and subsequently sensitive only to the density and ionization fields. However, it is possible that heating is never "complete" in this sense before the completion of reionization, meaning neutral pockets of IGM gas may remain at temperatures at or below $T_{\rm CMB}$ until they are engulfed in the overlap event of large ionized bubbles.

D. Reionization: As the global star formation rate density climbs, the growth of ionized regions around groups and clusters of galaxies will continue, eventually culminating in the completion of cosmic reionization. This rise in ionization corresponds to a decline in the amount of neutral hydrogen in the Universe capable of producing or absorbing 21-cm radiation. As a result, the amplitude of the 21-cm signal, both in its mean and fluctuations, falls as reionization progresses.

The evolution of 21-cm fluctuations is more complicated, though this same series of events imprints on fluctuation patterns as well.

2.4.2 Sensitivity to Model Parameters

Use this section to highlight the sensitivity to parameters in more detail.

Things to discuss:

- Sensitivity to $T_{\rm min}$ and f_*.
- Sensitivity to α_X, $E_{\rm min}$, and f_X.
- Sensitivity to ζ and $R_{\rm mfp}$ (and updates)
- Clumping, feedback
- Shot noise in galaxy counts in voxels.
- PopIII stuff. AGN stuff.
- Exotic physics? Defer to Jonathan's chapter.

2.4.3 Modeling Tools

Predictions from previous section came from a mix of different groups and codes. Discuss some differences here.

- 21CMFAST and DEXM
- Anastasia's code
- simfast21
- ARES
- RT simulations

Bibliography

[1]

[2] T. Abel, M. L. Norman, and P. Madau. Photon-conserving Radiative Transfer around Point Sources in Multidimensional Numerical Cosmology. *ApJ*, 523:66–71, September 1999.

[3] Rennan Barkana and Abraham Loeb. Detecting the Earliest Galaxies through Two New Sources of 21 Centimeter Fluctuations. *ApJ*, 626(1):1–11, Jun 2005.

[4] Gilles Chabrier. Galactic Stellar and Substellar Initial Mass Function. *PASP*, 115(809):763–795, Jul 2003.

[5] X. Chen and J. Miralda-Escudé. The Spin-Kinetic Temperature Coupling and the Heating Rate due to Lyα Scattering before Reionization: Predictions for 21 Centimeter Emission and Absorption. *ApJ*, 602:1–11, February 2004.

[6] Asantha Cooray and Ravi Sheth. Halo models of large scale structure. *Physics Reports*, 372(1):1–129, Dec 2002.

[7] Arpan Das, Andrei Mesinger, Andrea Pallottini, Andrea Ferrara, and John H. Wise. High-mass X-ray binaries and the cosmic 21-cm signal: impact of host galaxy absorption. *MNRAS*, 469(1):1166–1174, Jul 2017.

[8] John J. Eldridge and Elizabeth R. Stanway. Spectral population synthesis including massive binaries. *MNRAS*, 400(2):1019–1028, Dec 2009.

[9] G. Fabbiano. Populations of X-Ray Sources in Galaxies. *ARAA*, 44(1):323–366, Sep 2006.

[10] G. B. Field. Excitation of the Hydrogen 21-CM Line. *Proceedings of the IRE*, 46:240–250, January 1958.

[11] M. Fukugita and M. Kawasaki. Reionization during Hierarchical Clustering in a Universe Dominated by Cold Dark Matter. *MNRAS*, 269:563, August 1994.

[12] S. R. Furlanetto and J. R. Pritchard. The scattering of Lyman-series photons in the intergalactic medium. *MNRAS*, 372:1093–1103, November 2006.

[13] Steven Furlanetto, Matias Zaldarriaga, and Lars Hernquist. The Growth of HII Regions During Reionization. *arXiv.org*, March 2004.

[14] Steven R. Furlanetto. The global 21-centimeter background from high redshifts. *MNRAS*, 371(2):867–878, Sep 2006.

[15] Steven R Furlanetto and Samuel Johnson Stoever. Secondary ionization and heating by fast electrons. *Monthly Notices of the Royal Astronomical Society*, 404:1869, June 2010.

[16] M. Gilfanov, H. J. Grimm, and R. Sunyaev. L_X-SFR relation in star-forming galaxies. *MNRAS*, 347(3):L57–L60, Jan 2004.

[17] Christopher M Hirata. Wouthuysen-Field coupling strength and application to high-redshift 21-cm radiation. *MNRAS*, 367(1):259–274, March 2006.

[18] Pavel Kroupa. On the variation of the initial mass function. *MNRAS*, 322(2):231–246, Apr 2001.

[19] Claus Leitherer, Daniel Schaerer, Jeffrey D. Goldader, Rosa M. González Delgado, Carmelle Robert, Denis Foo Kune, Duília F. de Mello, Daniel Devost, and Timothy M. Heckman. Starburst99: Synthesis Models for Galaxies with Active Star Formation. *ApJS*, 123(1):3–40, Jul 1999.

[20] Piero Madau, Avery Meiksin, and Martin J. Rees. 21 Centimeter Tomography of the Intergalactic Medium at High Redshift. *ApJ*, 475(2):429–444, Feb 1997.

[21] Matthew McQuinn. Constraints on X-ray emissions from the reionization era. *MNRAS*, 426(2):1349–1360, Oct 2012.

[22] S. Mineo, M. Gilfanov, and R. Sunyaev. X-ray emission from star-forming galaxies - II. Hot interstellarmedium. *MNRAS*, 426(3):1870–1883, Nov 2012.

[23] I. F. Mirabel, M. Dijkstra, P. Laurent, A. Loeb, and J. R. Pritchard. Stellar black holes at the dawn of the universe. *A&A*, 528:A149, Apr 2011.

[24] Jordan Mirocha, Richard H. Mebane, Steven R. Furlanetto, Krishma Singal, and Donald Trinh. Unique signatures of Population III stars in the global 21-cm signal. *MNRAS*, 478(4):5591–5606, Aug 2018.

[25] Jordan Mirocha, Stephen Skory, Jack O Burns, and John H Wise. Optimized Multi-frequency Spectra for Applications in Radiative Feedback and Cosmological Reionization. *The Astrophysical Journal*, 756(1):94, September 2012.

[26] S. Peng Oh. Reionization by Hard Photons. I. X-Rays from the First Star Clusters. *ApJ*, 553(2):499–512, Jun 2001.

[27] Jonathan R Pritchard and Steven R Furlanetto. Descending from on high: Lyman-series cascades and spin-kinetic temperature coupling in the 21-cm line. *MNRAS*, 367(3):1057–1066, April 2006.

[28] Ronald A. Remillard and Jeffrey E. McClintock. X-ray properties of black-hole binaries. *Annual Review of Astronomy and Astrophysics*, 44(1):49–92, 2006.

[29] Edwin E. Salpeter. The Luminosity Function and Stellar Evolution. *ApJ*, 121:161, Jan 1955.

[30] John Scalo. The IMF Revisited: A Case for Variations. In Gary Gilmore and Debbie Howell, editors, *The Stellar Initial Mass Function (38th Herstmonceux Conference)*, volume 142 of *Astronomical Society of the Pacific Conference Series*, page 201, Jan 1998.

[31] J M Shull and M E van Steenberg. X-ray secondary heating and ionization in quasar emission-line clouds. *The Astrophysical Journal*, 298:268, November 1985.

[32] Elizabeth R. Stanway, J. J. Eldridge, and George D. Becker. Stellar population effects on the inferred photon density at reionization. *MNRAS*, 456(1):485–499, Feb 2016.

[33] Takamitsu L. Tanaka, Ryan M. O'Leary, and Rosalba Perna. The imprint of the cosmic supermassive black hole growth history on the 21 cm background radiation. *MNRAS*, 455(3):2619–2626, Jan 2016.

[34] Max Tegmark, Joseph Silk, Martin J. Rees, Alain Blanchard, Tom Abel, and Francesco Palla. How Small Were the First Cosmological Objects? *ApJ*, 474:1, Jan 1997.

[35] Rajat M Thomas and Saleem Zaroubi. Time-evolution of ionization and heating around first stars and miniqsos. *Monthly Notices of the Royal Astronomical Society*, 384(3):1080–1096, March 2008.

[36] J. Wolcott-Green and Z. Haiman. Feedback from the infrared background in the early Universe. *MNRAS*, 425(1):L51–L55, Sep 2012.

[37] S. A. Wouthuysen. On the excitation mechanism of the 21-cm (radio-frequency) interstellar hydrogen emission line. *AJ*, 57:31–32, 1952.

[38] B Zygelman. Hyperfine Transitions in Atomic Hydrogen. *ApJ*, 622:1356–1362, 2005.

Chapter 3

Chapter title

Author Name

Abstract

This chapter discusses some important things

3.1 A Section

Lorem ipsum dolor sit amet, consectetur adipiscing elit. Duis eu egestas erat. Maecenas tincidunt lacinia tincidunt. Mauris id lectus nec neque feugiat condimentum vitae at diam. In vel orci nunc, non commodo mauris. Vivamus ipsum enim, vulputate quis pharetra non, molestie quis felis. Vivamus porttitor placerat turpis at accumsan. Nunc tortor velit, faucibus a rhoncus nec, blandit non elit. Nam consectetur lectus eu nisi blandit dapibus rhoncus dui tempus. Mauris fermentum dolor vel ipsum vulputate sit amet ultricies tortor lacinia. Donec ut nibh erat. Morbi nec mi ante. Integer nec vestibulum diam. Donec tincidunt pellentesque quam, ut interdum mauris venenatis condimentum. Nam condimentum, augue in aliquet gravida, neque dui elementum eros, id semper eros purus sed felis. Curabitur in justo sit amet sapien ultrices hendrerit at quis nibh. Quisque iaculis pulvinar tincidunt.

$$\begin{aligned} C(12) &= \left[\overrightarrow{\pi}\cdot\overrightarrow{\phi}\,(x+r)\right] \\ &\approx 1-\text{const}\frac{r^2}{L^2}\int_r^L\frac{x\mathrm{d}x}{x^2}+\cdots \\ &\approx 1-\text{const}\frac{r^2}{L^2}\ln\frac{x\mathrm{d}x}{x^2}+\cdots . \end{aligned} \tag{3.1}$$

Aenean tellus risus, porta sit amet porta vitae, tincidunt ut felis. Class aptent taciti sociosqu ad litora torquent per conubia nostra, per inceptos himenaeos. Vestibulum ante ipsum primis in faucibus orci luctus et ultrices posuere cubilia Curae; Phasellus pulvinar placerat velit auctor egestas. Vivamus euismod fringilla tincidunt. Sed ut magna felis, id sollicitudin nunc. Quisque a dui eu erat consectetur egestas a quis justo. Aenean euismod congue diam, vel posuere urna fermentum sit amet. Lorem ipsum dolor sit amet, consectetur adipiscing

Figure 3.1: This is figure 1 in chapter 1.

Table 3.1: Greek Letters.

α	β	γ	δ	ε	ε	ζ	η
θ	ϑ	γ	κ	λ	μ	ν	ξ
o	π	ϖ	ρ	ρ	σ	ς	
τ	υ	ϕ	φ	χ	ψ	ω	
Γ	Δ	Θ	Λ	Ξ	Π	Σ	Υ
Φ	Ψ	Ω					

elit. Mauris faucibus lacus eget est mollis auctor. Donec at nibh ligula, et posuere massa. Phasellus quis leo diam [1]. Donec aliquam blandit risus, eu venenatis ante euismod eu. Curabitur cursus justo id arcu condimentum feugiat. Integer sapien urna, vulputate et adipiscing nec, convallis et justo. Suspendisse in ipsum at felis ornare interdum [2],

Cras adipiscing sagittis nunc vel luctus. Suspendisse volutpat augue quis erat semper consequat dignissim tellus euismod. Morbi hendrerit, tellus id aliquam iaculis, nibh leo tincidunt eros, vitae varius ligula felis in mi.

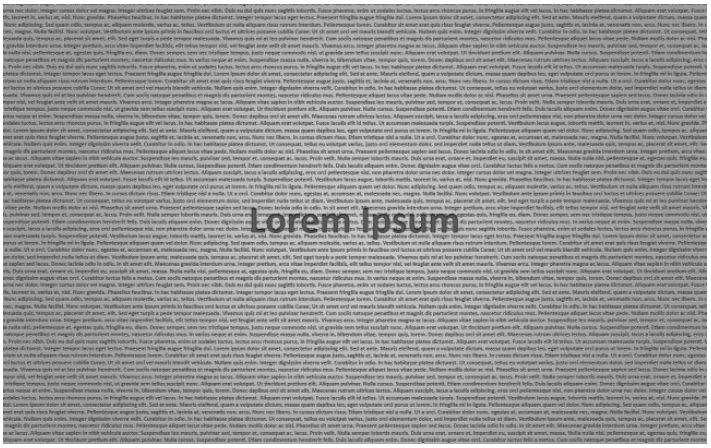

Figure 3.2: This is figure 2 in chapter 1.

Bibliography

[1] KI Diamantaras and SY Kung. *Principal component neural networks: theory and applications*. John Wiley & Sons, Inc. New York, NY, USA, 1996.

[2] D. Tulone and S. Madden. PAQ: Time Series Forecasting for Approximate Query Answering in Sensor Networks. In *Proceedings of the 3rd European Workshop on Wireless Sensor Networks*, pages 21–37. Springer, 2006.

Chapter 4

Chapter title

Author Name

Abstract

This chapter discusses some important things

4.1 A Section

Lorem ipsum dolor sit amet, consectetur adipiscing elit. Duis eu egestas erat. Maecenas tincidunt lacinia tincidunt. Mauris id lectus nec neque feugiat condimentum vitae at diam. In vel orci nunc, non commodo mauris. Vivamus ipsum enim, vulputate quis pharetra non, molestie quis felis. Vivamus porttitor placerat turpis at accumsan. Nunc tortor velit, faucibus a rhoncus nec, blandit non elit. Nam consectetur lectus eu nisi blandit dapibus rhoncus dui tempus. Mauris fermentum dolor vel ipsum vulputate sit amet ultricies tortor lacinia. Donec ut nibh erat. Morbi nec mi ante. Integer nec vestibulum diam. Donec tincidunt pellentesque quam, ut interdum mauris venenatis condimentum. Nam condimentum, augue in aliquet gravida, neque dui elementum eros, id semper eros purus sed felis. Curabitur in justo sit amet sapien ultrices hendrerit at quis nibh. Quisque iaculis pulvinar tincidunt.

$$\begin{aligned} C(12) &= \left[\overrightarrow{\pi}\cdot\overrightarrow{\phi}\,(x+r)\right] \\ &\approx 1-\text{const}\frac{r^2}{L^2}\int_r^L\frac{x\mathrm{d}x}{x^2}+\cdots \\ &\approx 1-\text{const}\frac{r^2}{L^2}\ln\frac{x\mathrm{d}x}{x^2}+\cdots . \end{aligned} \tag{4.1}$$

Aenean tellus risus, porta sit amet porta vitae, tincidunt ut felis. Class aptent taciti sociosqu ad litora torquent per conubia nostra, per inceptos himenaeos. Vestibulum ante ipsum primis in faucibus orci luctus et ultrices posuere cubilia Curae; Phasellus pulvinar placerat velit auctor egestas. Vivamus euismod fringilla tincidunt. Sed ut magna felis, id sollicitudin nunc. Quisque a dui eu erat consectetur egestas a quis justo. Aenean euismod congue diam, vel posuere urna fermentum sit amet. Lorem ipsum dolor sit amet, consectetur adipiscing

Figure 4.1: This is figure 1 in chapter 1.

Table 4.1: Greek Letters.

α	β	γ	δ	ε	ε	ζ	η
θ	ϑ	γ	κ	λ	μ	ν	ξ
o	π	ϖ	ρ	ρ	σ	ς	
τ	υ	ϕ	φ	χ	ψ	ω	
Γ	Δ	Θ	Λ	Ξ	Π	Σ	Υ
Φ	Ψ	Ω					

elit. Mauris faucibus lacus eget est mollis auctor. Donec at nibh ligula, et posuere massa. Phasellus quis leo diam [1]. Donec aliquam blandit risus, eu venenatis ante euismod eu. Curabitur cursus justo id arcu condimentum feugiat. Integer sapien urna, vulputate et adipiscing nec, convallis et justo. Suspendisse in ipsum at felis ornare interdum [2],

Cras adipiscing sagittis nunc vel luctus. Suspendisse volutpat augue quis erat semper consequat dignissim tellus euismod. Morbi hendrerit, tellus id aliquam iaculis, nibh leo tincidunt eros, vitae varius ligula felis in mi.

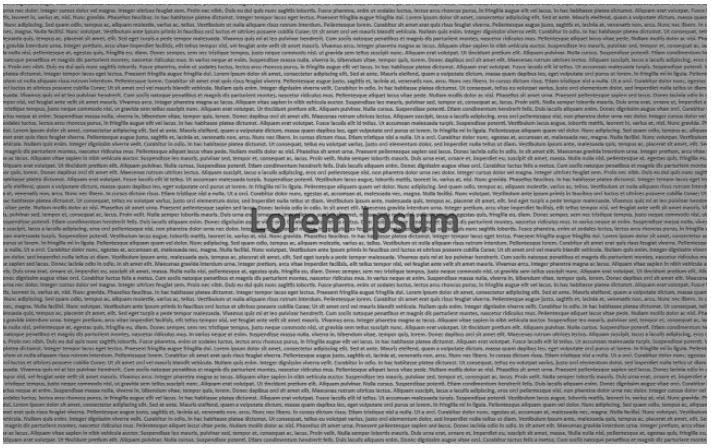

Figure 4.2: This is figure 2 in chapter 1.

Bibliography

[1] KI Diamantaras and SY Kung. *Principal component neural networks: theory and applications*. John Wiley & Sons, Inc. New York, NY, USA, 1996.

[2] D. Tulone and S. Madden. PAQ: Time Series Forecasting for Approximate Query Answering in Sensor Networks. In *Proceedings of the 3rd European Workshop on Wireless Sensor Networks*, pages 21–37. Springer, 2006.

Chapter 5

Chapter title

Author Name

Abstract

This chapter discusses some important things

5.1 A Section

Lorem ipsum dolor sit amet, consectetur adipiscing elit. Duis eu egestas erat. Maecenas tincidunt lacinia tincidunt. Mauris id lectus nec neque feugiat condimentum vitae at diam. In vel orci nunc, non commodo mauris. Vivamus ipsum enim, vulputate quis pharetra non, molestie quis felis. Vivamus porttitor placerat turpis at accumsan. Nunc tortor velit, faucibus a rhoncus nec, blandit non elit. Nam consectetur lectus eu nisi blandit dapibus rhoncus dui tempus. Mauris fermentum dolor vel ipsum vulputate sit amet ultricies tortor lacinia. Donec ut nibh erat. Morbi nec mi ante. Integer nec vestibulum diam. Donec tincidunt pellentesque quam, ut interdum mauris venenatis condimentum. Nam condimentum, augue in aliquet gravida, neque dui elementum eros, id semper eros purus sed felis. Curabitur in justo sit amet sapien ultrices hendrerit at quis nibh. Quisque iaculis pulvinar tincidunt.

$$\begin{aligned} C(12) &= \left[\overrightarrow{\pi}\cdot\overrightarrow{\phi}\,(x+r)\right] \\ &\approx 1-\text{const}\frac{r^2}{L^2}\int_r^L\frac{x\mathrm{d}x}{x^2}+\cdots \\ &\approx 1-\text{const}\frac{r^2}{L^2}\ln\frac{x\mathrm{d}x}{x^2}+\cdots . \end{aligned} \tag{5.1}$$

Aenean tellus risus, porta sit amet porta vitae, tincidunt ut felis. Class aptent taciti sociosqu ad litora torquent per conubia nostra, per inceptos himenaeos. Vestibulum ante ipsum primis in faucibus orci luctus et ultrices posuere cubilia Curae; Phasellus pulvinar placerat velit auctor egestas. Vivamus euismod fringilla tincidunt. Sed ut magna felis, id sollicitudin nunc. Quisque a dui eu erat consectetur egestas a quis justo. Aenean euismod congue diam, vel posuere urna fermentum sit amet. Lorem ipsum dolor sit amet, consectetur adipiscing

Figure 5.1: This is figure 1 in chapter 1.

Table 5.1: Greek Letters.

α	β	γ	δ	ε	ε	ζ	η
θ	ϑ	γ	κ	λ	μ	ν	ξ
o	π	ϖ	ρ	ρ	σ	ς	
τ	υ	ϕ	φ	χ	ψ	ω	
Γ	Δ	Θ	Λ	Ξ	Π	Σ	Υ
Φ	Ψ	Ω					

elit. Mauris faucibus lacus eget est mollis auctor. Donec at nibh ligula, et posuere massa. Phasellus quis leo diam [1]. Donec aliquam blandit risus, eu venenatis ante euismod eu. Curabitur cursus justo id arcu condimentum feugiat. Integer sapien urna, vulputate et adipiscing nec, convallis et justo. Suspendisse in ipsum at felis ornare interdum [2],

Cras adipiscing sagittis nunc vel luctus. Suspendisse volutpat augue quis erat semper consequat dignissim tellus euismod. Morbi hendrerit, tellus id aliquam iaculis, nibh leo tincidunt eros, vitae varius ligula felis in mi.

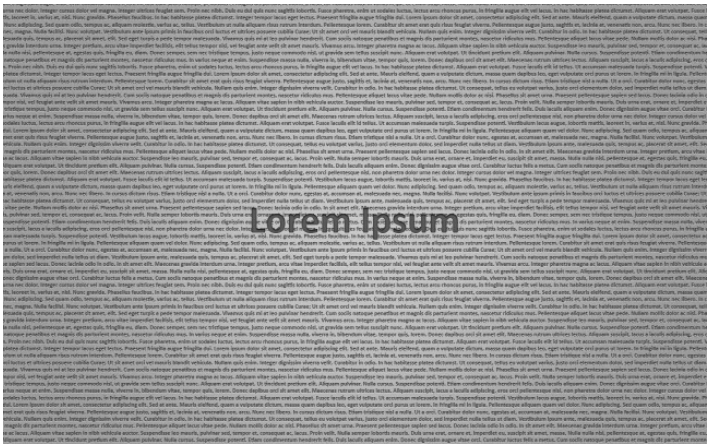

Figure 5.2: This is figure 2 in chapter 1.

Bibliography

[1] KI Diamantaras and SY Kung. *Principal component neural networks: theory and applications*. John Wiley & Sons, Inc. New York, NY, USA, 1996.

[2] D. Tulone and S. Madden. PAQ: Time Series Forecasting for Approximate Query Answering in Sensor Networks. In *Proceedings of the 3rd European Workshop on Wireless Sensor Networks*, pages 21–37. Springer, 2006.

Chapter 6

Chapter title

Author Name

Abstract

This chapter discusses some important things

6.1 A Section

Lorem ipsum dolor sit amet, consectetur adipiscing elit. Duis eu egestas erat. Maecenas tincidunt lacinia tincidunt. Mauris id lectus nec neque feugiat condimentum vitae at diam. In vel orci nunc, non commodo mauris. Vivamus ipsum enim, vulputate quis pharetra non, molestie quis felis. Vivamus porttitor placerat turpis at accumsan. Nunc tortor velit, faucibus a rhoncus nec, blandit non elit. Nam consectetur lectus eu nisi blandit dapibus rhoncus dui tempus. Mauris fermentum dolor vel ipsum vulputate sit amet ultricies tortor lacinia. Donec ut nibh erat. Morbi nec mi ante. Integer nec vestibulum diam. Donec tincidunt pellentesque quam, ut interdum mauris venenatis condimentum. Nam condimentum, augue in aliquet gravida, neque dui elementum eros, id semper eros purus sed felis. Curabitur in justo sit amet sapien ultrices hendrerit at quis nibh. Quisque iaculis pulvinar tincidunt.

$$\begin{aligned} C(12) &= \left[\overrightarrow{\pi}\cdot\overrightarrow{\phi}\,(x+r)\right] \\ &\approx 1-\text{const}\frac{r^2}{L^2}\int_r^L\frac{x\mathrm{d}x}{x^2}+\cdots \\ &\approx 1-\text{const}\frac{r^2}{L^2}\ln\frac{x\mathrm{d}x}{x^2}+\cdots . \end{aligned} \tag{6.1}$$

Aenean tellus risus, porta sit amet porta vitae, tincidunt ut felis. Class aptent taciti sociosqu ad litora torquent per conubia nostra, per inceptos himenaeos. Vestibulum ante ipsum primis in faucibus orci luctus et ultrices posuere cubilia Curae; Phasellus pulvinar placerat velit auctor egestas. Vivamus euismod fringilla tincidunt. Sed ut magna felis, id sollicitudin nunc. Quisque a dui eu erat consectetur egestas a quis justo. Aenean euismod congue diam, vel posuere urna fermentum sit amet. Lorem ipsum dolor sit amet, consectetur adipiscing

Figure 6.1: This is figure 1 in chapter 1.

Table 6.1: Greek Letters.

α	β	γ	δ	ε	ε	ζ	η
θ	ϑ	γ	κ	λ	μ	ν	ξ
o	π	ϖ	ρ	ρ	σ	ς	
τ	υ	ϕ	φ	χ	ψ	ω	
Γ	Δ	Θ	Λ	Ξ	Π	Σ	Υ
Φ	Ψ	Ω					

elit. Mauris faucibus lacus eget est mollis auctor. Donec at nibh ligula, et posuere massa. Phasellus quis leo diam [1]. Donec aliquam blandit risus, eu venenatis ante euismod eu. Curabitur cursus justo id arcu condimentum feugiat. Integer sapien urna, vulputate et adipiscing nec, convallis et justo. Suspendisse in ipsum at felis ornare interdum [2],

Cras adipiscing sagittis nunc vel luctus. Suspendisse volutpat augue quis erat semper consequat dignissim tellus euismod. Morbi hendrerit, tellus id aliquam iaculis, nibh leo tincidunt eros, vitae varius ligula felis in mi.

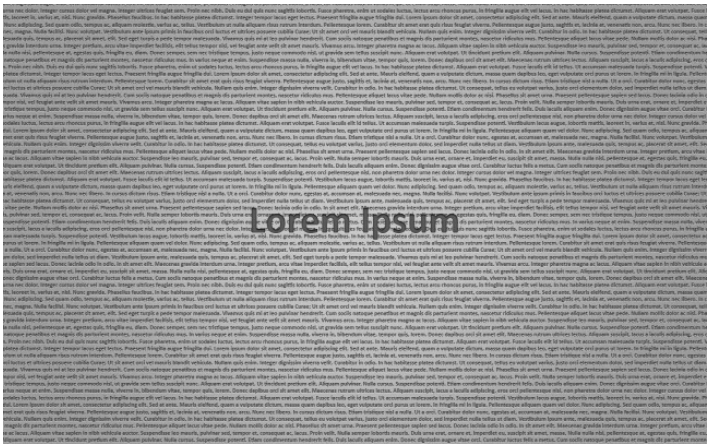

Figure 6.2: This is figure 2 in chapter 1.

Bibliography

[1] KI Diamantaras and SY Kung. *Principal component neural networks: theory and applications*. John Wiley & Sons, Inc. New York, NY, USA, 1996.

[2] D. Tulone and S. Madden. PAQ: Time Series Forecasting for Approximate Query Answering in Sensor Networks. In *Proceedings of the 3rd European Workshop on Wireless Sensor Networks*, pages 21–37. Springer, 2006.

Chapter 7

Chapter title

Author Name

Abstract

This chapter discusses some important things

7.1 A Section

Lorem ipsum dolor sit amet, consectetur adipiscing elit. Duis eu egestas erat. Maecenas tincidunt lacinia tincidunt. Mauris id lectus nec neque feugiat condimentum vitae at diam. In vel orci nunc, non commodo mauris. Vivamus ipsum enim, vulputate quis pharetra non, molestie quis felis. Vivamus porttitor placerat turpis at accumsan. Nunc tortor velit, faucibus a rhoncus nec, blandit non elit. Nam consectetur lectus eu nisi blandit dapibus rhoncus dui tempus. Mauris fermentum dolor vel ipsum vulputate sit amet ultricies tortor lacinia. Donec ut nibh erat. Morbi nec mi ante. Integer nec vestibulum diam. Donec tincidunt pellentesque quam, ut interdum mauris venenatis condimentum. Nam condimentum, augue in aliquet gravida, neque dui elementum eros, id semper eros purus sed felis. Curabitur in justo sit amet sapien ultrices hendrerit at quis nibh. Quisque iaculis pulvinar tincidunt.

$$\begin{aligned} C(12) &= \left[\overrightarrow{\pi}\cdot\overrightarrow{\phi}\,(x+r)\right] \\ &\approx 1-\text{const}\frac{r^2}{L^2}\int_r^L\frac{x\mathrm{d}x}{x^2}+\cdots \\ &\approx 1-\text{const}\frac{r^2}{L^2}\ln\frac{x\mathrm{d}x}{x^2}+\cdots . \end{aligned} \tag{7.1}$$

Aenean tellus risus, porta sit amet porta vitae, tincidunt ut felis. Class aptent taciti sociosqu ad litora torquent per conubia nostra, per inceptos himenaeos. Vestibulum ante ipsum primis in faucibus orci luctus et ultrices posuere cubilia Curae; Phasellus pulvinar placerat velit auctor egestas. Vivamus euismod fringilla tincidunt. Sed ut magna felis, id sollicitudin nunc. Quisque a dui eu erat consectetur egestas a quis justo. Aenean euismod congue diam, vel posuere urna fermentum sit amet. Lorem ipsum dolor sit amet, consectetur adipiscing

Figure 7.1: This is figure 1 in chapter 1.

Table 7.1: Greek Letters.

α	β	γ	δ	ε	ε	ζ	η
θ	ϑ	γ	κ	λ	μ	ν	ξ
o	π	ϖ	ρ	ρ	σ	ς	
τ	υ	ϕ	φ	χ	ψ	ω	
Γ	Δ	Θ	Λ	Ξ	Π	Σ	Υ
Φ	Ψ	Ω					

elit. Mauris faucibus lacus eget est mollis auctor. Donec at nibh ligula, et posuere massa. Phasellus quis leo diam [1]. Donec aliquam blandit risus, eu venenatis ante euismod eu. Curabitur cursus justo id arcu condimentum feugiat. Integer sapien urna, vulputate et adipiscing nec, convallis et justo. Suspendisse in ipsum at felis ornare interdum [2],

Cras adipiscing sagittis nunc vel luctus. Suspendisse volutpat augue quis erat semper consequat dignissim tellus euismod. Morbi hendrerit, tellus id aliquam iaculis, nibh leo tincidunt eros, vitae varius ligula felis in mi.

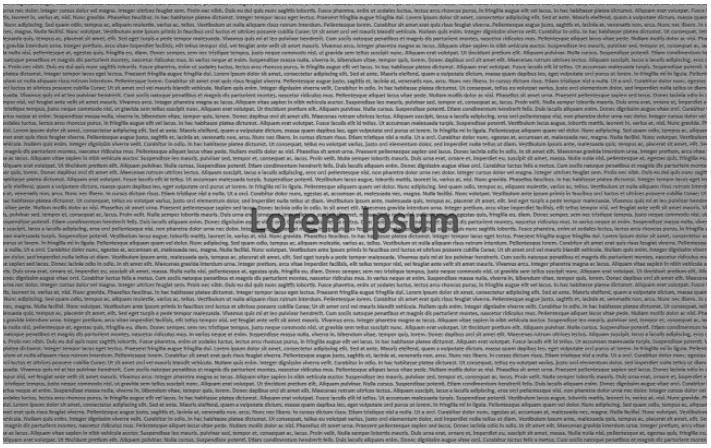

Figure 7.2: This is figure 2 in chapter 1.

Bibliography

[1] KI Diamantaras and SY Kung. *Principal component neural networks: theory and applications*. John Wiley & Sons, Inc. New York, NY, USA, 1996.

[2] D. Tulone and S. Madden. PAQ: Time Series Forecasting for Approximate Query Answering in Sensor Networks. In *Proceedings of the 3rd European Workshop on Wireless Sensor Networks*, pages 21–37. Springer, 2006.

Chapter 8

Chapter title

Author Name

Abstract

This chapter discusses some important things

8.1 A Section

Lorem ipsum dolor sit amet, consectetur adipiscing elit. Duis eu egestas erat. Maecenas tincidunt lacinia tincidunt. Mauris id lectus nec neque feugiat condimentum vitae at diam. In vel orci nunc, non commodo mauris. Vivamus ipsum enim, vulputate quis pharetra non, molestie quis felis. Vivamus porttitor placerat turpis at accumsan. Nunc tortor velit, faucibus a rhoncus nec, blandit non elit. Nam consectetur lectus eu nisi blandit dapibus rhoncus dui tempus. Mauris fermentum dolor vel ipsum vulputate sit amet ultricies tortor lacinia. Donec ut nibh erat. Morbi nec mi ante. Integer nec vestibulum diam. Donec tincidunt pellentesque quam, ut interdum mauris venenatis condimentum. Nam condimentum, augue in aliquet gravida, neque dui elementum eros, id semper eros purus sed felis. Curabitur in justo sit amet sapien ultrices hendrerit at quis nibh. Quisque iaculis pulvinar tincidunt.

$$\begin{aligned} C(12) &= \left[\overrightarrow{\pi}\cdot\overrightarrow{\phi}\,(x+r)\right] \\ &\approx 1-\text{const}\frac{r^2}{L^2}\int_r^L\frac{x\mathrm{d}x}{x^2}+\cdots \\ &\approx 1-\text{const}\frac{r^2}{L^2}\ln\frac{x\mathrm{d}x}{x^2}+\cdots . \end{aligned} \tag{8.1}$$

Aenean tellus risus, porta sit amet porta vitae, tincidunt ut felis. Class aptent taciti sociosqu ad litora torquent per conubia nostra, per inceptos himenaeos. Vestibulum ante ipsum primis in faucibus orci luctus et ultrices posuere cubilia Curae; Phasellus pulvinar placerat velit auctor egestas. Vivamus euismod fringilla tincidunt. Sed ut magna felis, id sollicitudin nunc. Quisque a dui eu erat consectetur egestas a quis justo. Aenean euismod congue diam, vel posuere urna fermentum sit amet. Lorem ipsum dolor sit amet, consectetur adipiscing

Figure 8.1: This is figure 1 in chapter 1.

Table 8.1: Greek Letters.

α	β	γ	δ	ε	ε	ζ	η
θ	ϑ	γ	κ	λ	μ	ν	ξ
o	π	ϖ	ρ	ρ	σ	ς	
τ	υ	ϕ	φ	χ	ψ	ω	
Γ	Δ	Θ	Λ	Ξ	Π	Σ	Υ
Φ	Ψ	Ω					

elit. Mauris faucibus lacus eget est mollis auctor. Donec at nibh ligula, et posuere massa. Phasellus quis leo diam [1]. Donec aliquam blandit risus, eu venenatis ante euismod eu. Curabitur cursus justo id arcu condimentum feugiat. Integer sapien urna, vulputate et adipiscing nec, convallis et justo. Suspendisse in ipsum at felis ornare interdum [2],

Cras adipiscing sagittis nunc vel luctus. Suspendisse volutpat augue quis erat semper consequat dignissim tellus euismod. Morbi hendrerit, tellus id aliquam iaculis, nibh leo tincidunt eros, vitae varius ligula felis in mi.

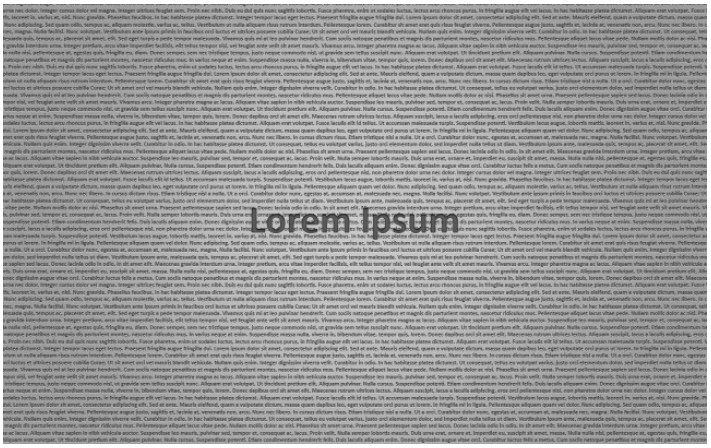

Figure 8.2: This is figure 2 in chapter 1.

Bibliography

[1] KI Diamantaras and SY Kung. *Principal component neural networks: theory and applications*. John Wiley & Sons, Inc. New York, NY, USA, 1996.

[2] D. Tulone and S. Madden. PAQ: Time Series Forecasting for Approximate Query Answering in Sensor Networks. In *Proceedings of the 3rd European Workshop on Wireless Sensor Networks*, pages 21–37. Springer, 2006.